Available online at www.sciencedirect.com
ScienceDirect
Journal of Hydrodynamics
2015,27(6):919-933
DOI: 10.1016/S1001-6058(15)60555-8
www.sciencedirect.com/
science/journal/l0016058

Hydrodynamics of the interceptor on a 2-D flat plate by CFD and experiments*

MANSOORI M.[1], FERNANDES A. C.[2]
1. Department of Naval and Ocean Engineering, Federal University of Rio de Janeiro, RJ, Brazil,
E-mail: mkerend2004@gmail.com
2. Department of Naval and Ocean Engineering, Federal University of Rio de Janeiro, RJ, Brazil

(Received October 7, 2014, Revised November 11, 2015)

Abstract: Nowadays, the use of interceptor by both partial and total dynamic lift crafts is quite common. In this article, a lot of evidence is given regarding the effectiveness of interceptor. The interceptor, when placed at the stern region, changes the pressure distribution around the craft. Its presence affects drag force, lifting force and the position of pressure's center leading to a new trim. This study focuses on hydrodynamic effects of interceptors on a 2-D flat plate based on both computational fluid dynamic (CFD) and experimental approaches. The Reynolds average Navier-Stokes (RANS) equations are used to model the flow around a fixed flat plate with an interceptor at different heights and attack angles. Based on finite volume method and SIMPLE algorithm which uses static structures, this model can be analyzed and the RANS results can be compared with the experimental data obtained in the current channel of the laboratory of waves and current of COPPE/UFRJ (LOC in Portuguese acronym). According to the results, the increase of pressure at the end of the flat plate was proportional to the interceptor height. In addition, the existence of interceptors can significantly increase the lift force coefficient at high angles of attack also proportional to the interceptor height. The presence of interceptor at the end of the flat plate increased both the lift coefficient and the drag coefficient but hydrodynamic drag did not grow as fast as the lift coefficient did. The lift coefficient increased much more. Furthermore, the results showed that the interceptor effectiveness is proportional to the boundary layer thickness at the end of the flat plate. As the interceptor was inside the boundary layer alterations of flow speed led to changes in boundary layer thickness, directly affecting interceptor's efficiency. Optimum choice of interceptor height had a great effect on its efficiency, and in choosing it the flow speed and length of the boat must be taken into consideration.

Key words: interceptor, craft, 2-D flat plate, lifting coefficient, Reynolds average Navier-Stokes (RANS), pressure distribution, computational fluid dynamic, drag

Introduction

The interceptor is composed of a thin vertical plate usually perpendicular to the craft hull and located near the stern. The major role of the interceptor is to apply an overpressure enough to lift the stern, which leads to change of the craft's trim. Figure 1 shows the outline of an interceptor implementation at the aft of a planing craft.

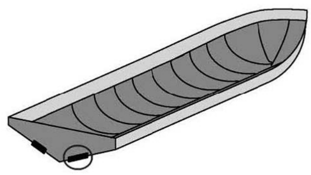

Fig.1 The implementation of an interceptor at the aft of a planing craft

The dynamic instabilities like progressive heeling, trimming, and chine walking, unstable pitching and rolling-induced parametrically[1,2] may show up. The occurrence of proposing instabilities is also possible[3]. Nevertheless, due to presence of the interceptor, the pressure distribution, which is changed by the craft movement, leads to the variation of draft, trim and possibly the control of the mentioned instabilities. Traditionally, the trim control tools are located at the stern

* **Biography:** MANSOORI M. (1984-), Male, Ph. D., Postdoctoral Researcher

region of the craft including flaps, T-hydrofoils, trim tabs, interceptors with vertical blades, plates, and wedge-shaped components. Former studies mostly covered the design factors such as the position of gravity load center, the forward speed, and other geometric parameters of the planing hull regarding the craft movement[4-6]. In the case of the controllable appendages, research efforts are made by Karafiath and Fisher[7] and Molini and Brizolara[8] introduced a very simple potential flow model for the prediction of pressure and lift force in front of the interceptors. Tsai and Hawing[9] examined the effect of trim mechanisms (interceptors, stern flap and the integration of both) on resistance decrease. The outcomes of the experiment verified that the resistance of the planing craft and the running trim can be reduced by a well-designed trim mechanism. Furthermore, they realized that the best resistance reduction corresponds to the Froude numbers between 2.0 and 2.5 using both interceptor and stern flap. Peláez et al.[10] performed a preliminary computational fluid dynamic (CFD) simulation to find the best angle for stern flap at every speed of the boat. The outcomes refer to a great increase of efficiency (vertical force to drag force). Later on in this article, there is evidence about Reynolds average Navier-Stokes (RANS) equations and 2-D flat plate models, which are upright to the flow[11] and have attack angle[12]. In general, the interceptors are reliable equipment for eliminating craft trim problems and controlling them. The implementations of these methods are also considered by designers when the high-pressure region at the bow causes the bow-up phenomenon[12,13]. For the first time, a series of model tests to compare and determine the roles of interceptor and trim tab was suggested by Maritime Dynamics Institute (MDI)[14] with interceptors with different heights but the same span size. By means of the tests, the hydrodynamic advantages of interceptors over trim tab at different heights have become clear. The effect of hydrodynamic interceptors on fast crafts was investigated by Ghassemi and Mansoori[15] to find their optimum geometrical characteristic based on numerical method. Their results showed that the interceptor causes an intense pressure rate in its contact point.

Therefore, the positive effects of an interceptor on the trim instabilities have been made clear. The main goals of the present study are to get deep understanding of why an interceptor can help and when an interceptor can be useless by a 2-D flat plate which is simulated and experimented with receptors at different heights. The RANS equations[16] model the flow around the fixed flat with and without an interceptor. This model is analyzed based on finite volume method and SIMPLE algorithm in Fluent computational software package[17].

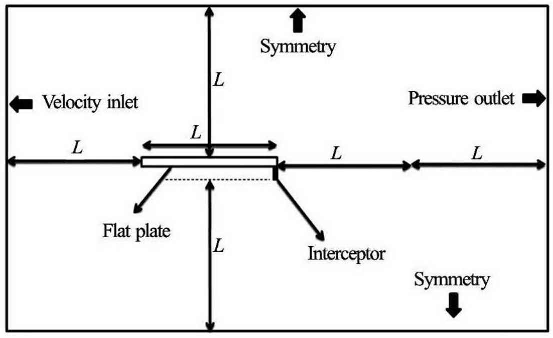

Fig.2 Shape of the simulation domain of the flow, dimension are in terms of L

1. The CFD domain

This section describes the CFD domain. It is composed of a semi-infinite region, the fluid extends sidewise up to extreme borders. However, these extreme borders are so farther away that they do not affect the flow around the flat plate. Appropriate determination of computational domain around the flat plate, which is located on the boundary layer, can unquestionably lead to more accurate computational results. The simulation domain and boundary conditions are shown in Fig.2. The conditions at a symmetry boundary are: (1) no flow across the boundary and (2) no scalar flux across the boundary.

2. Governing equations

Two different approaches can be used to deal with this kind of device, one is numerical and the other is experimental. On the other hand, there are several numerical procedures, although the main ones used in naval sector are the panel model or the RANS codes. The panel model makes it possible to solve the potential flow around the hull, but it is not suitable for the evolution of the effect of viscosity including separation when the interceptor is present. Furthermore, the interceptor operates within the boundary layer where the flow is highly viscous. The present work uses RANS codes, which are based on the numerical solution of the Navier-Stokes equations.

2.1 *RANS equations*

Most fluid flows, especially in the sea, are turbulent. The most common equations for numerical simulation of turbulent flow, as already mentioned, are RANS equations with a turbulence modeling. RANS equations are universally adaptive control equations of kinematics in viscous fluid. RANS equations can be written as follows[16]

$$\rho\frac{\partial(u_i u_j)}{\partial X_j}+\rho\frac{\partial(u_i)}{\partial t}=-\frac{\partial p}{\partial X_i}+$$

$$\frac{\partial}{\partial X_i}\left[\mu_0\left(\frac{\partial u_i}{\partial X_j}+\frac{\partial u_j}{\partial X_i}\right)-\frac{2}{3}\mu_0\frac{\partial u_i}{\partial X_i}\delta_{ij}-\rho\overline{u_i' u_j'}\right]\rho f_i \tag{1}$$

where u_i and u_j are time-average speed components $(i,j=1,2,3)$, p is time-average pressure, ρ represents the density of water, μ_0 is viscosity coefficient of water, f_i is mass force and $\rho\overline{u_i' u_j'}$ is Reynolds stress. If we introduce a general variable ϕ the conservative form of all fluid flow equations, can usefully be written in the following form

$$\frac{\partial(\rho\phi)}{\partial t}+\mathrm{div}(\rho\phi u)=\mathrm{div}(\Gamma\,\mathrm{grad}\,\phi)+S_\phi \tag{2}$$

The Eq.(2) is the so-called transport equation for property ϕ, where Γ is the diffusion coefficient and S_ϕ is the source. The velocity field in RANS equations must, of course, also satisfy the mass conservation (continuity) equation, which can be obtained by Eq.(3) as follows

$$\frac{\partial}{\partial X}(\rho u)+\frac{\partial}{\partial y}(\rho v)=0 \tag{3}$$

By solving this set of equations using the SIMPLE algorithm (see below), the unknown variables will be determined.

2.2 *The k-ε model equations*

Following the pros and cons of different turbulence models[16], the simplest method, which has less time convergence, is the k-ε method. The k-ε model[17] has two model equations, one for k and one for ε, based on the best understanding of the relevant processes that cause changes in these variables. In this work k and ε are used to define respectively the representative scales of velocity θ and length l of the large-scale turbulence as follows

$$\theta=k^{1/2},\quad l=\frac{k^{3/2}}{\varepsilon} \tag{4}$$

Applying the same approach as in the mixing length model, we specify the eddy velocity as follows

$$\mu_t=C\rho\theta l=\rho C_\mu\frac{k^2}{\varepsilon} \tag{5}$$

where C_μ is a dimensionless constant. The standard model uses the following transport equations for k and ε:

$$\frac{\partial(\rho k)}{\partial t}+\mathrm{div}(\rho k U)=\mathrm{div}\left(\frac{\mu_t}{\sigma_k}\mathrm{grad}k\right)+2\mu_t E_{ij}E_{ij}-\rho\varepsilon \tag{6a}$$

$$\frac{\partial(\rho\varepsilon)}{\partial t}+\mathrm{div}(\rho\varepsilon U)=\mathrm{div}\left(\frac{\mu_t}{\sigma_\varepsilon}\mathrm{grad}\varepsilon\right)+$$

$$C_{1\varepsilon}\frac{\varepsilon}{k}2\mu_t E_{ij}E_{ij}-C_{1\varepsilon}\rho\frac{\varepsilon^2}{k} \tag{6b}$$

and Ref.[18]

$$2\mu_t E_{ij}=2\mu_t\,\mathrm{div}U \tag{7}$$

In words, the Eq.(6) may be put in the form

Rate of change of k or ε +

Transport of k or ε by convection =

Transport of k or ε by diffusion +

Rate of production of k or ε −

Rate of destruction of k or ε

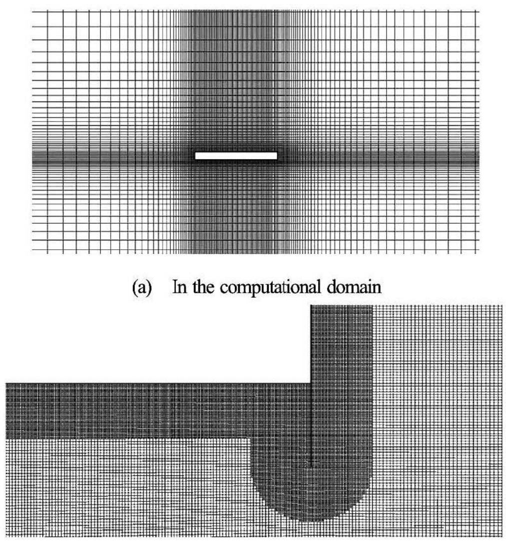

Fig.3 A sample of the generated grid

Table 1 The independence of the grid to the elements number by calculating the lift coefficient for several angles of attack

The element numbers of the grid	Lift coefficient (C_L)		
	$\alpha = 3^{\circ}$	$\alpha = 6^{\circ}$	$\alpha = 9^{\circ}$
80 000 elements	0.2732	0.6034	0.9107
115 000 elements	0.2974	0.6276	0.9434
125 000 elements	0.3221	0.6413	0.9824
130 000 elements	0.3224	0.6446	0.9832
For flat plate in small attack $C_L = 2\pi\alpha$ angle	0.3286	0.6573	0.9859

Note: α is the angle of attack.

Table 2 The verification study for resistance of flat plate with interceptor at a Reynolds number of 300 000

Grids	Refinement ratio	Convergence ratio	P	Grid uncertainly %
2, 4, 6	$2^{0.5}$	0.43	0.44	3.48
1, 3, 5	$2^{0.5}$	0.29	0.95	3.10
4, 5, 6	$2^{0.5}$	0.79	0.10	73.00
3, 4, 5	$2^{0.5}$	0.65	0.49	5.80
2, 3, 4	$2^{0.5}$	0.52	1.20	6.20
1, 2, 3	$2^{0.5}$	0.41	1.60	3.50

Note: P is thedistance metric of the asymptotic rang, Coarsest grid 6 with 5 803 points to the finest grid 1 with 130 000 points.

The equations contain five adjustable constants $C_{\mu}\sigma_k$, $\sigma_{\varepsilon} C_{1\varepsilon}$ and $C_{2\varepsilon}$. The standard k-ε model employs the following values for constants that are obtained by comprehensive data fitting for a wide range of turbulent flows:

$$C_{\mu} = 0.09\ ,\ \ \sigma_k = 1.0\ ,\ \ \sigma_{\varepsilon} = 1.3\ ,$$

$$C_{\varepsilon 1} = 1.44\ ,\ \ C_{\varepsilon 2} = 1.92$$

These values are well justified in Ref.[18] and verified by the results below, they are adequate for the present investigation.

In this study, the turbulence equations are coupled with RANS equations. It implies that the two equations of turbulence model are added to the set of governing equations. Thereby, by solving six equations simultaneously, the accuracy will improve[18]. It is notable to mention that the flow around flat plate is laminar, but the turbulence model is just applied for the small region around the interceptor because the interceptor creates vortex flow in front of itself.

3. Solver

The solver, in the presented paper, is based on the finite volume method. The finite volume method was developed as a special finite difference method. It consists of three main steps[18]:

(1) Integration of the governing equations of fluid flow over all the control volumes of the solution domain.

(2) Conversion of the integral equations into a system of algebraic equations by discretization of integrated equation of the flow processes such as convection, diffusion and sources. The discretization consists of substitution of a variety of finite-difference-type approximations in the integrated equations.

(3) Solution of the algebraic equations using an iterative method.

To obtain the pressure and velocity profiles, the RANS and turbulence equations are numerically solved. Firstly, the discretized equations are derived by finite volume method. Secondly, they are solved by the SIMPLE[18] method and Implicit Pressure-Correction method which are respectively used for flow equations and pressure equations.

4. Grid generation

The first step for grid generating within the finite volume method is to divide the domain into discrete control volumes. We place a number of nodal points in the space between our geometrical margins. The boundaries (or faces) of control volumes are positioned mid-way between adjacent nodes. Thus, each node is surrounded by a control volume or cell. It is common practice to set up control volumes near the edge of the domain in such a way that the physical boundaries coincide with the control volume boundaries. Furthermore, the grid should be able to analyze the separation, stagnation point regions and boundary layers. The last one is critical in the present case. Figure 3 shows a sample of the generated grid around the flat plate of the present work.

An appropriate grid should contain control volumes that should be near the edge of domain to cover thoroughly the boundaries of the model and the separation, the stagnation points and boundary layers should also be able to be analyzed by the grid. The wall function is an analytical treatment for the first cell near the wall where the velocity vector and all other scalar quantities are extrapolated from the known quantities on the wall boundary surface. The two layers wall function model is a model that imposes a first thin linear layer near the wall and a second logarithmic layer over the first. This model assumes that the centroid of the first cell near the wall lies within the logarithmic region of the boundary layer. The wall treatment is optimized to compute a mesh with a $y^+ < 50$.

As mentioned above, it is important to provide the arranged elements in the generated grid around the body, especially when there is a boundary layer in the simulation area, because the boundary layer simulation is strongly dependent on the grid quality. The number of elements is an important factor in grid quality. Higher number of elements leads to more accurate results up to a limit, which is a compromise point between processing time and accuracy. Table 1 summarizes the study that has been performed in the present work. The independency of the results for the lift coefficients is clear from it. Table 2 shows the verification study for resistance of flat plate with interceptor by the factors of safety method[19].

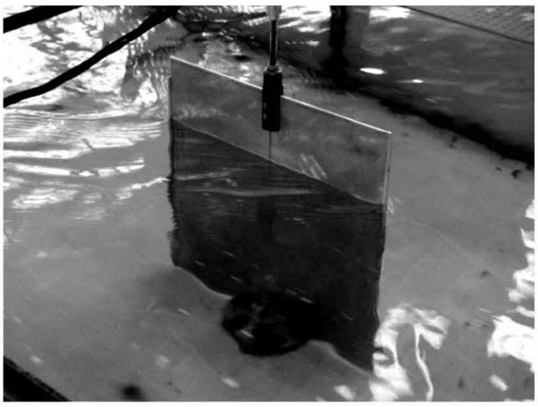

Fig.4(a) The model of flat plate at the LOC

Fig.4(b) 0.005 m interceptor at the end of the flat plate

5. Experimental setup

The experimental tests have been performed in LOC (Laboratório de Ondas e Correntes, Laboratory of Waves and Current) of COPPE, Federal University of Rio de Janeiro. The current channel (22 m long, 1.4 m wide, and 0.5 m deep) allows a maximum speed of 0.5 m/s in the test section. This corresponds to depth Froude number less than 0.225. The former was used for the tests with the 2-D flat plate. The experimental set-up allows the measurements of forces, moments and the center of pressure for different angles of flow incidence and different interceptor heights. Figure 4(a) shows the flat plate model that is used in LOC. The ratio of plate thickness to length is 0.001, that is, very thin. Figure 4(b) shows clearly the 0.005 m ($d/L = 0.005$) interceptor at the end of the flat plate. The dynamometer placed on the top of the flat plate was powered by a voltage source. The small gap in the bottom and low deformation of the free surface assures the infinite wing (2-D) characteristics. This was confirmed several times[20].

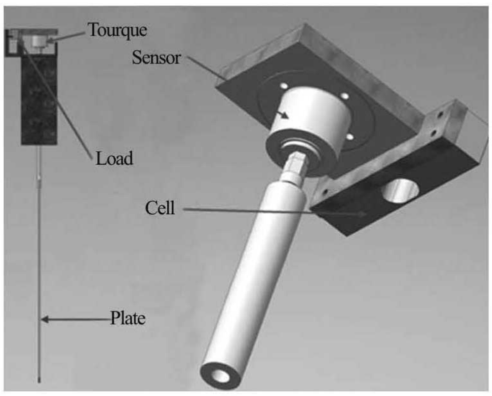

Fig.5 Assembly details of the torque sensor and load cell

The experimental apparatus was mounted in accordance with the details shown in Fig.5. A load cell and a torque sensor were positioned at the top of the plate. These sensors were calibrated before positioned in the apparatus.

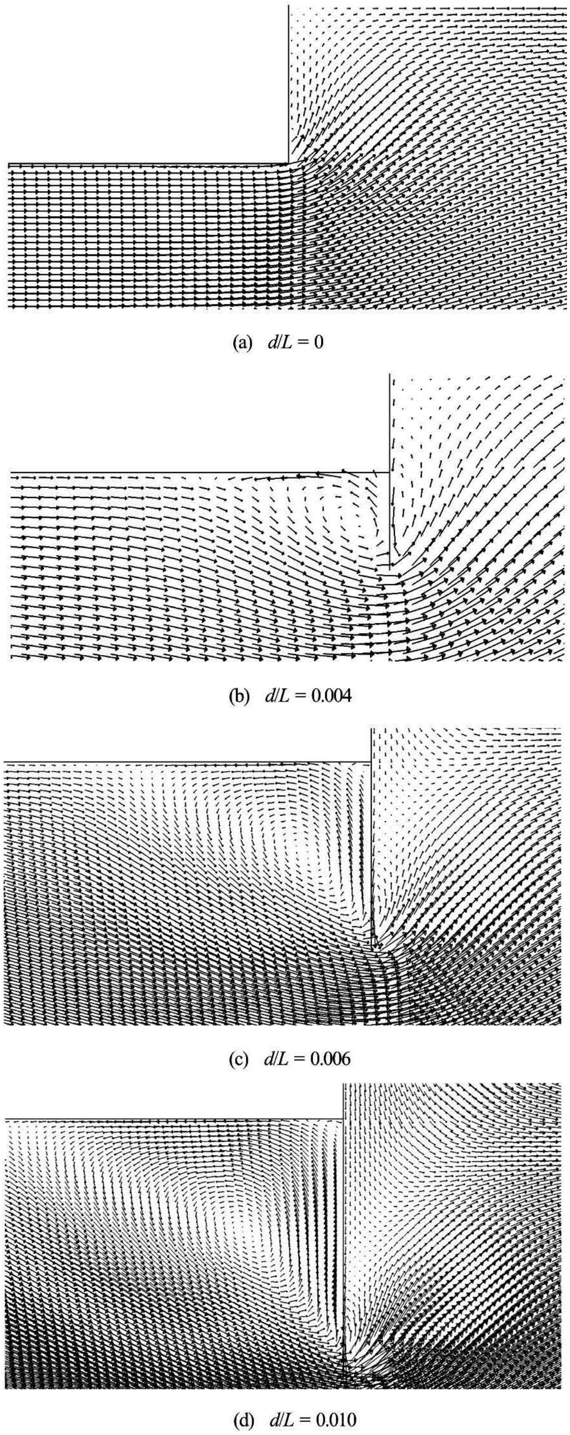

(a) $d/L = 0$

(b) $d/L = 0.004$

(c) $d/L = 0.006$

(d) $d/L = 0.010$

Fig.6 Flow vectors around the flat plate, where d and L are the interceptor height and the flat plate length respectively

The vortex shedding frequencies for the static flat plate were obtained through spectral analysis of the signal acquired from an acoustic Doppler velocimeter (ADV), which was positioned at a point in the wake of the plate. The velocity of the current flowing in the channel was obtained from a turbine type flow- meter. The data acquisition from the load cell was performed using a system (NI-9172 module in conjunction with the universal NI Daq-219) which has A/D converters and customized connections for the straingauges bridge complement required for the cell. The digital signal was recorded by software built in Lab View 8.2. The acquisition of data from the torque sensor was performed similarly, but using an analog signal conditioner that amplifies and filters the signal before being digitalized.

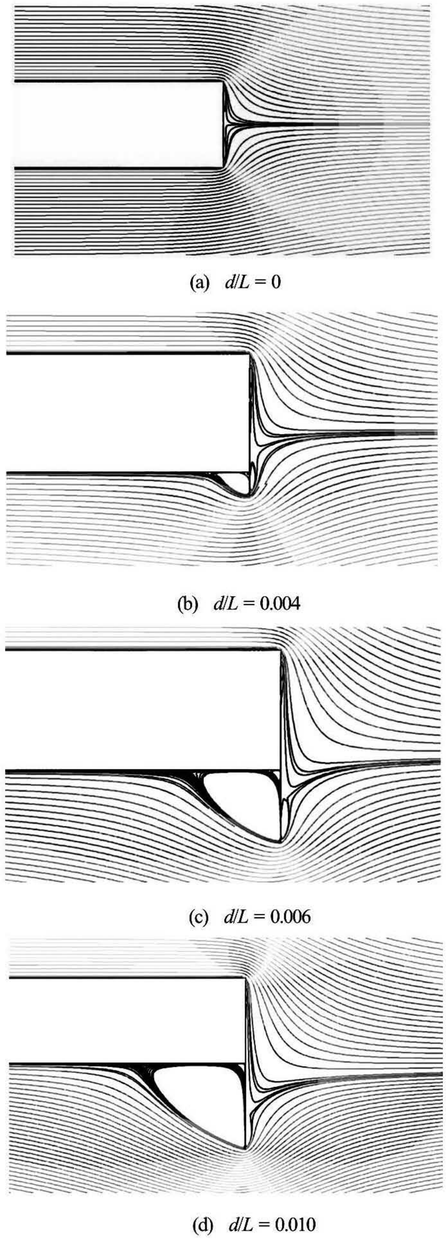

(a) $d/L = 0$

(b) $d/L = 0.004$

(c) $d/L = 0.006$

(d) $d/L = 0.010$

Fig.7 Streamlines around the flat plate

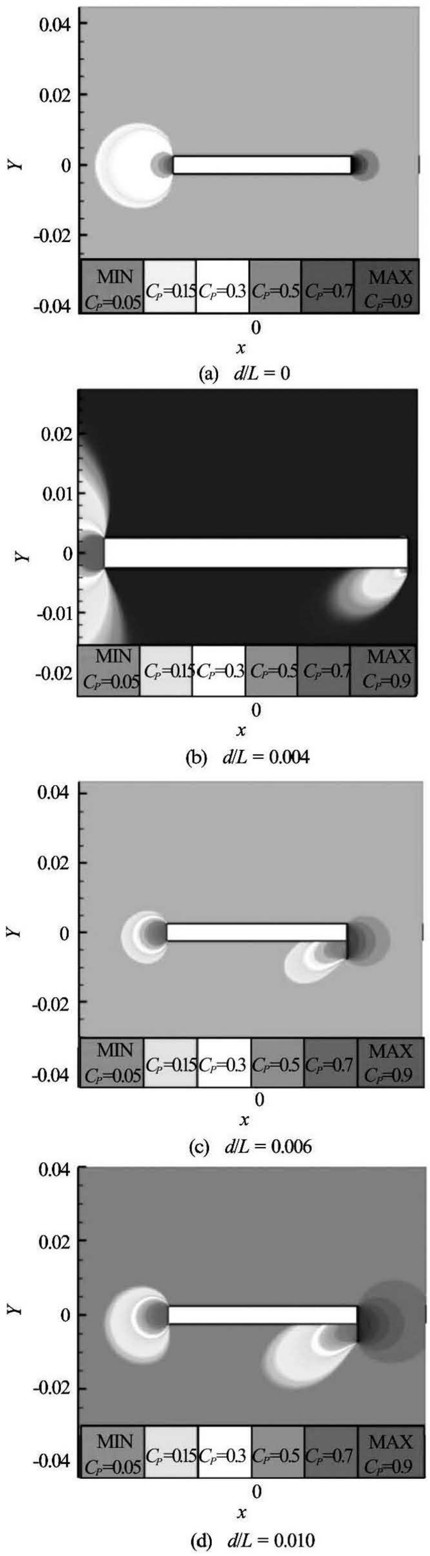

Fig.8 Pressure contours around the flat plate

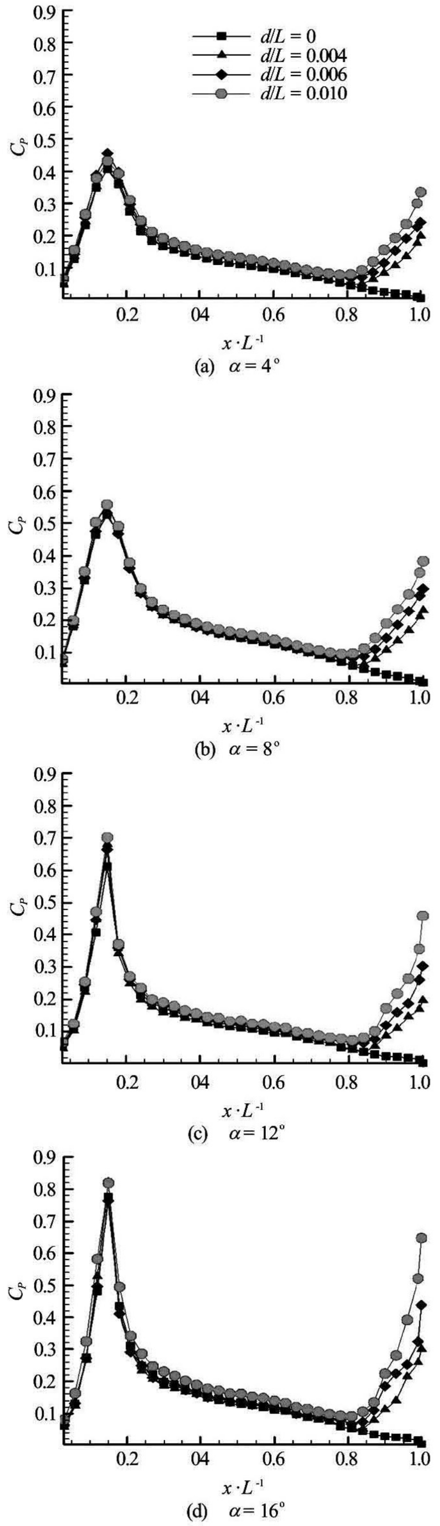

Fig.9 Pressure distribution at the bottom of the flat plate at various attack angles with and without interceptor at different heights, note that the x-axis corresponds to the position along the flat plate, that is from 0 to $x/L = 1.0$ (interceptor position)

6. The results of 2-D flat plate outcomes

In this part, findings from the CFD simulation and from experiments in LOC are compared. Figures

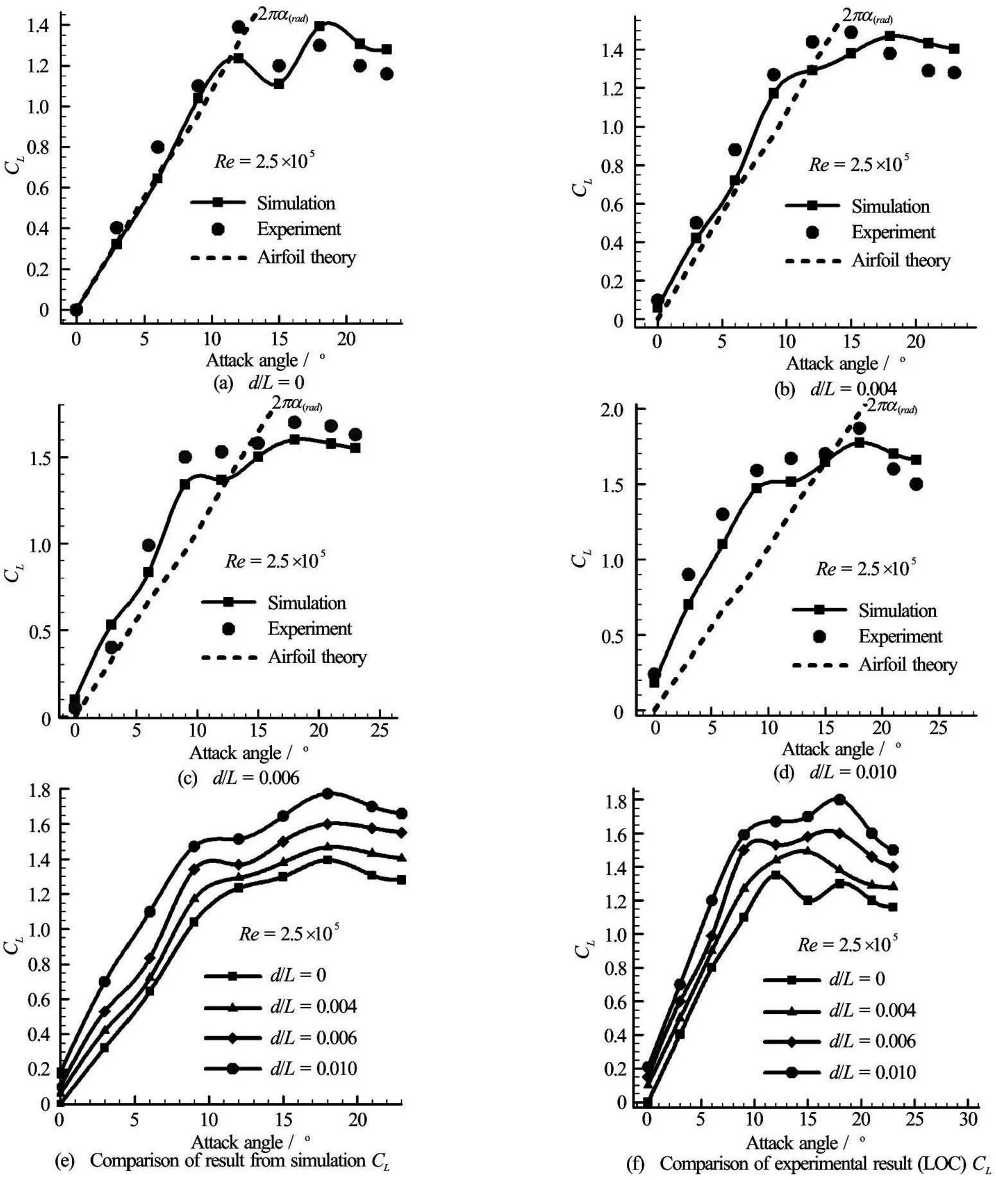

Fig.10 Lifting force coefficient for the flat plate. Figures 10(a)-10(d) includes the analytical result from infinite wing potential theory $(2\pi\alpha_{(rad)})$, with $\alpha_{(rad)}$ in radians

below include the changes of flow vector around interceptors with several heights, the effect of interceptor on lift and drag force of the plate, and also the effect of interceptor's height on the position of the center of pressure.

The bottom of a high speed craft is almost flat, hence the present study can be simplified, and we will illustrate what happens locally there. Later on, in the present work, the effect of boundary layer's thickness on interceptor's efficiency is studied. The study can help us to make the best choice for interceptors' height.

In Fig.6, flow vectors, representing the local velocity intensity and direction, are shown around the flat plate without interceptor (Fig.6(a)) and with interceptor at different heights (Figs.6(b)-6(d)). According to these Figures, a strong stationary vortex is formed in front of the interceptor. At the back of the interceptor, there are also vortices now mainly due to separation.

In Fig.7, the streamlines in the boundary layer around the flat plate without interceptor (Fig.7(a)) and with interceptor (Figs.7(b)-7(d)) are shown. In the case of the flat plate without interceptor, of course there is no vortex at the end of the flat plate (where the interceptor will be) (Fig.7(a)) but in the case of the flat plate with interceptor a front vortex is formed as a result of the contact of fluid flow with the vertical obstacle and it is shown in Fig.7(d), when the interceptor is $d/L = 0.01$ (0.005 m height). As it will be

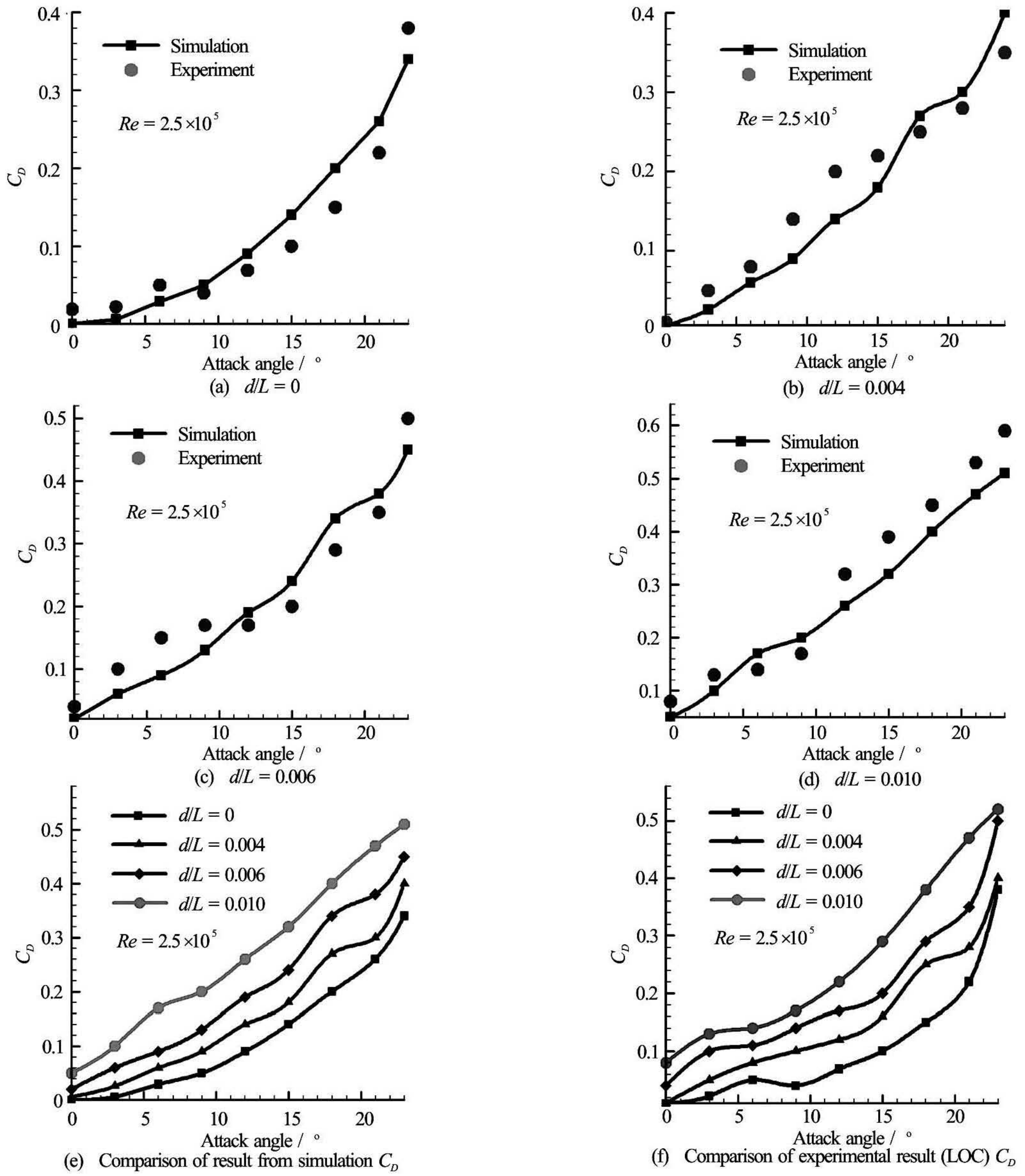

Fig.11 Drag force coefficient for the flat plate

demonstrated later, this front vortex increases the pressure at the end of the flat plate as a result of which the center of pressure moves toward the end of the plate and this, by itself, can decrease the trim. As vortices get more intense, the interceptor height increases accordingly, the force at the end of the plate before the interceptor will also increase as the height increases.

Figure 8 shows pressure contour around the even plate with (Figs.8(b)-8(d)) and without (Fig.8(a)) interceptor. The maximum pressure occurres at the stagnation point (Fig.8(a)). From the stagnation point toward the end of the plate, the pressure intensity decreases and according to Figs.8(b)-8(d), with interceptor, pressure distribution changes at the end of the plate and this increase of pressure ratio is proportionate to the height of interceptor. This pressure increase can significantly change the lifting forces and cause

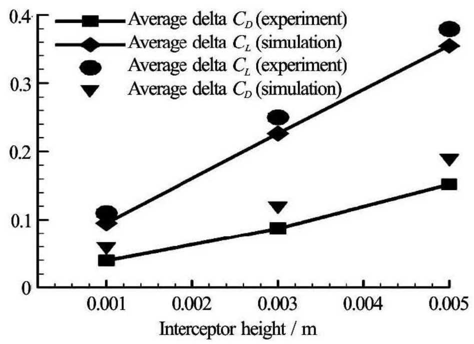

Fig.12 Average increase of C_L and C_D versus interceptor height (d) at several angles of attack in the range between 0° and 15°

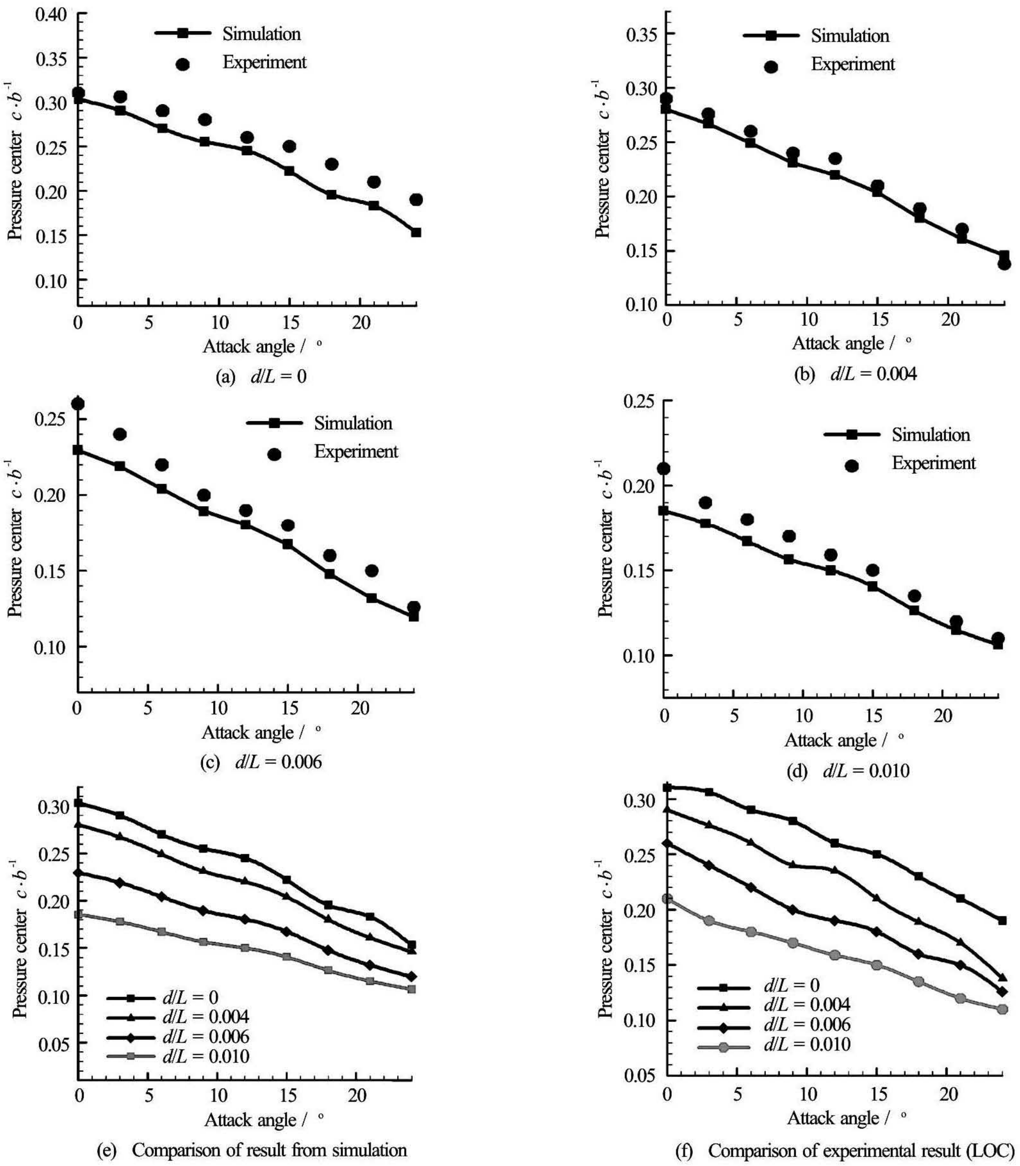

Fig.13 Center of pressure position for the flat plate

better control, which will be considered in the following parts.

Now, the results in Fig.9 show that without interceptor, the pressure distribution toward the end of the flat plate decreases. This reduction of pressure distribution is the main cause of trim in vessels. In addition, they show that the presence of the interceptor causes a stagnation region with consequent pressure increase. As the pressure increases, so does the height of interceptor, and conversely, trim angle decreases. The significant advantage of this pressure increase at the bottom of the vessel is the creation of lifting force, which decreases wetted surface in a more uniform way. It also changes the drag force, but the frictional resistance decreases by the reduction of wetted surface.

Next, in Fig.10 the lift coefficient in different angles of attack for the flat plate is studied, with and without interceptor. As it is clear from Figs.10(a)-10(d), the experimental and simulation results are quite close to each other, which is quite positive for validation purposes of both methodologies. The above results indicate that the presence of interceptor leads to an increase of the lift force coefficient (Figs.10(e), 10(f)). They also show that the higher the interceptor, the stall angle happens for slightly smaller angles as in the case of hydrofoils with camber. This increase of lift force coefficient follows the increase of the height of the interceptor. As demonstrated in Fig.8, this lift increase is caused due to the shift in pressure distribution at the end of the flat plate. When the craft is actually floating on the sea, this increase of coefficient in lifting forces created by the interceptor can lead to a resistance decrease through reducing wetted surface. In fact, the most important feature of interceptors in high speed crafts is the increase of lift coefficient making the craft gets out of water more quickly.

Now, the effect of interceptor on drag force coefficient is demonstrated in Fig.11. Experimental results are compared with those from RANS equations simulation for the flat plate with and without interceptor at different heights (Figs.11(a)-11(d)). An increase in plate's angle of attack results in a rise in drag force coefficient, therefore there is a higher increase in the drag force coefficient. This rise of drag force follows the interceptor's height, as it is shown in Figs.11(e) and 11(f).

In this article, the flat plate is modeled as completely fixed. But it allows the prognostic that in the real movement of the craft with interceptor, due to the pressure's positive gradient at the end of the craft, a lifting force would be formed at the bottom of the craft and this, alone, reduces the wetted surface of the craft, and consequently the resistance as well. Also, the interceptor makes the craft pass the hump point easier.

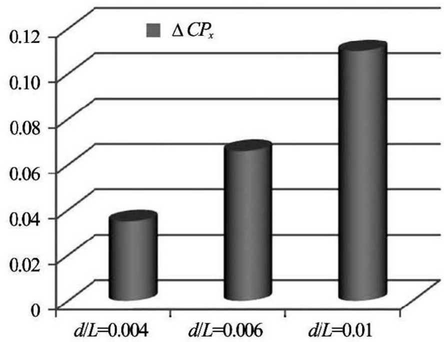

(a)

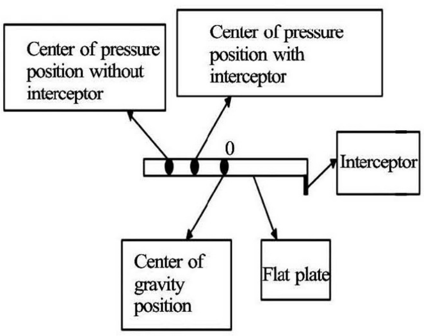

(b)

Fig.14 The effect of interceptor's height on the mean of distance decrease between the center of gravity and the center of pressure of the flat plate

Figure 12 has compared the mean of lift and drag coefficients increase caused by the interceptor with different heights. The presence of the interceptor at the end of the plate increases the lift coefficient and the drag coefficient, but the lift coefficient increases much more than the drag one.

In Fig.13, interceptor's effect on the position of the center of pressure is demonstrated. In these figures, both the RANS simulation and laboratory results (LOC) are compared for each case (Figs.13(a)-13(d)). The result is very favorable. In general, the distance created by hydrodynamic forces between the center of gravity and the center of pressure will produce a trim in the craft. Results from Figs.13(e) and 13(f) show that the interceptor pushes the center of pressure toward the plate's end. This reduction of distance may result in the decrease of trim in real crafts.

Figure 14 indicates the effect of the interceptor's height on mean decreases of the distance between the center of gravity and the center of pressure of the flat plate (Fig. 14(a)). In Fig.14 (b), an overall view of the flat plate and the interceptor and the change of position of the center of pressure toward the end of the flat plate is shown. This decrease of distance created by the interceptor is shown qualitatively in Fig.14(a). The maximum distance decrease is created by a 0.005 m $(d/L = 0.01)$ interceptor, which expresses the fact that the highest increase in pressure has occurred with maximum interceptor height.

7. Examining the effect of boundary layer thickness on interceptor's height (laminar flow)

Finally in this part, following Prof. Blount's suggestion[1] we will examine the effect of boundary layer thickness on the interceptor's efficiency. As it is indicated in previous parts, interceptor produces a lift force through creating a hydrodynamic pressure on the bottom of the plate, and despite this notable lift force, little hydrodynamic drag is generated. All conclusions discussed in previous sections are calculated in constant speed. Here, the relationship between the boundary layer thicknesses on interceptor's efficiency for various heights is investigated by changing the velocity of the flow. Also, the results from the simulation of the RANS equations are compared to outcomes of laboratory tests (LOC).

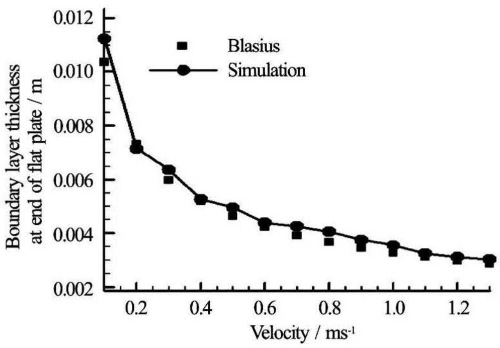

Fig.15(a) Boundary layer thickness for the flat plate versus velocity

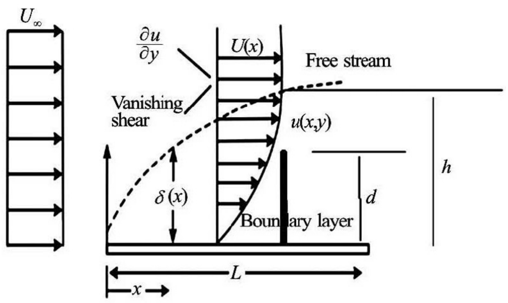

Fig.15(b) Boundary layer and free stream for flow over a flat plate

In Fig.15, the effect of flow speed on boundary layer thickness at the end of the plate, where interceptor is (Fig.15(a)) and flow profile in the boundary layer at the bottom of the flat plate (Fig.15(b)) is illustrated. The results from simulation are compared to Blasius' analytic formula[18] for the boundary layer thickness on the flat plate (Fig.15(a)). According to the results of Fig.15, a rise in the flow speed results in a decrease of the boundary layer thickness at the end of the plate; this drop shows a very important point.

When the flow velocity increases, for a given interceptor height, the ratio of d/h (where h is boundary layer thickness) increases. The contact speed to the interceptor increases because the interceptor is in the region of large boundary layer velocity gradient (Fig.15(b)). Figure 15(b) illustrates that there is initially a velocity gradient inside the boundary layer formed on the plate, in which speed increases move away. When the interceptor height reaches 0.6 of boundary layer thickness, the velocity is close to the flow velocity outside the boundary layer. The effect of these changes in the boundary layer on the interceptor's efficiency will be discussed later on.

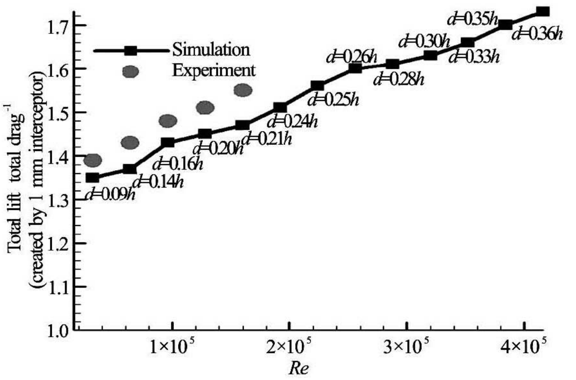

Fig.16 Total lift divided by total drag created by 0.001 m $(d/L = 0.0005)$ interceptor versus velocity. The result for LOC is limited because of the maximum velocity of the facility, the value d/h corresponds to ratio between the height of the interceptor and the boundary layer thickness at the end of the interceptor

In Fig.16, the ratio between the lift coefficient to drag coefficient created by 0.001 m $(d/L = 0.0005)$ interceptor with different Reynolds numbers is shown. The results from simulation are compared with experimental (LOC) ones, up to a speed of 0.5 m/s. As demonstrated in Fig.16, while the speed increases, the interceptor generates more lift force than drag force, and when the speed increases, the interceptor's height in the boundary layer increases as well. The maximum of lift force produced by the interceptor is calculated in highest studied speed, which is 1.2 m/s $(Re = 400\,000)$. For the interceptor with a 0.001 m height $(d/L = 0.0005)$, the maximum amount of d/h coefficient is 0.36, showing this important point that the interceptor is in the boundary layer at the beginning of velocity gradient, and the contact speed of fluid flow with the interceptor is much less than flow speed out of the boundary layer.

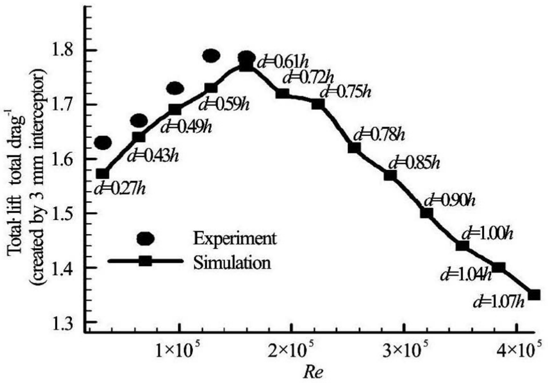

Fig.17 Total lift divided by total drag created by 0.003 m $(d/L = 0.001)$ interceptor versus Reynolds numbers. The result for LOC is limited because of the maximum velocity of the facility, the value d/h corresponds to ratio between the height of the interceptor and the boundary layer thickness at the end of the interceptor

In Fig.17, ratio of the lift to the drag produced by 0.003 m $(d/L = 0.001)$ interceptor in various Reynolds numbers is also shown. The ratio of lift force to drag force can be an appropriate relationship for evaluating interceptor's efficiency. As Fig.17 reveals, while interceptor's height is below 0.61 multiplied by boundary layer thickness, the proportion of lift force to drag force increases as speed rise. When the interceptor's height divided by boundary layer thickness is above 0.61, the drag force produced by the 0.003 m $(d/L = 0.001)$ interceptor increases, leading to a drop in the interceptor's output. This drag increase is caused by the interceptor height advancing in boundary layer velocity gradient. When the interceptor height reaches 0.61 of the boundary layer thickness, it has been observed that the flow speed before the interceptor is almost equal to the flow speed out of the boundary layer. Due to speed limitation in the laboratory (maximum: 0.5 m/s), results from simulation are compared to those of laboratory (LOC) up to the speed of 0.5 m/s $(Re = 140\,000)$. When the velocity rise into the 0.003 m $(d/L = 0.001)$ interceptor, there is a rapid growth in drag force and less lift force is produced. Boundary layer thickness in this article is derived from RANS equations simulation and represents the space between the plate (velocity of zero) and the point in which the speed is equal to 0.99 of fluid speed in the entrance.

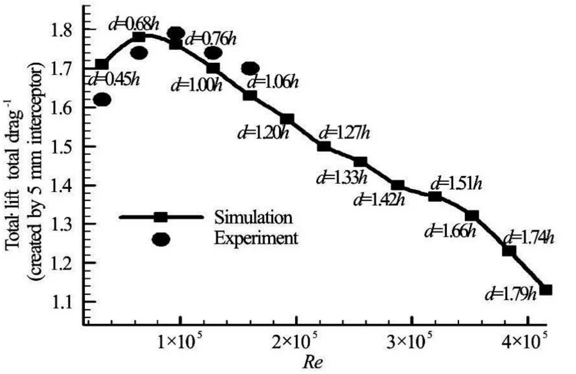

Fig.18 Total lift divided by total drag created by 0.005 m $(d/L = 0.006)$ interceptor versus Reynolds numbers. The result for LOC is limited because of the maximum velocity of the facility, the value d/h corresponds to the ratio of the height of the interceptor the boundary layer thickness at the end of the interceptor

In Fig.18, the proportion of lift force to drag force produced by 0.005 m $(d/L = 0.006)$ interceptor is illustrated. As we expected, the lift produced by a 0.005 m $(d/L = 0.006)$ interceptor is more than a 0.001 m (Fig.16) and 0.003 m (Fig.17), but with the speed increase and the boundary layer thickness decrease, the 0.005 m interceptor loses efficiency very fast. Again, when the interceptor's height reaches almost 0.6 of the boundary layer thickness, drag force has remarkably increased, resulting in the reduction of interceptor performance.

For a fixed length flat plate, increasing the free stream velocity of water flow increases the Reynolds number at the end of the flat plate. Increasing the Reynolds number for both laminar and turbulent flow will then reduce the calculated boundary layer thickness at the downstream end of the flat plate. As the velocity increases from zero at the surface of the plate, it becomes nearly equal to free stream velocity at about 0.6 of boundary layer thickness. From 0 to 0.6 of boundary layer thickness the drag of the interceptor (which is proportional to local velocity squared, V^2) is in a velocity gradient where V^2 is much lower than free stream velocity. When the height of the interceptor (d) is larger than about $0.6h$, the drag increases at greater rate. This can be observed in Figs.17-19. While drag is added, little additional lift is obtained. As demonstrated in Fig.19, up to the speed of 0.2 m/s $(Re = 40\,000)$ the best efficiency is recorded for the 0.005 m $(d/L = 0.006)$ interceptor, but by passing this speed, boundary layer thickness reduces and consequently the fall of ideal efficiency is viewed in this height. In the speed of 0.2 m/s, the 0.005 m $(d/L = 0.006)$ interceptor has passed 0.6 of boundary layer thickness (Fig.18) and drag has increased. Up to speed of 0.6 m/s $(Re = 150\,000)$, the best efficiency belongs to the interceptor with 0.003 m $(d/L = 0.001)$ height, but by passing this point, the 0.003 m $(d/L = 0.001)$ interceptor overtakes 0.6 of boundary layer thickness, and a profound shift occurs in the drag force, causing a fall in the 0.003 m interceptor output. A 0.001 m interceptor, due to its low height, will permanently be in the boundary layer velocity gradient (Fig.16) as the speed increases (above 0.8 m/s), and not much drag force is produced. As it is seen in Fig.18, the best interceptor performance in speeds above 0.8 m/s $(Re = 3\,000\,000)$ is acquired in the case of a 0.001 m $(d/L = 0.005)$ interceptor. Results of Fig.19 are briefly described in Table 3.

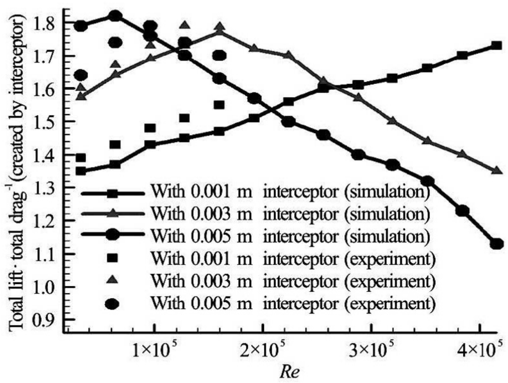

Fig.19 Comparison of the effect of Reynolds numbers on the interceptor effectiveness at different heights

Table 3 The effect of velocity on interceptor efficiency at various heights

Velocity/ $m \cdot s^{-1}$	0-0.4	0.4-0.6	0.6-0.8	0.8-1.2
Reynolds number	0- 1.5×10^5	1.5×10^5- 2×10^5	2×10^5- 3×10^5	3×10^5- 4×10^5
d/L				
0.0005	√∧	√∧	√√∧	√√√∧
0.0010	√√∧	√√√∧	√√√∨	√√∨
0.0060	√√√∧	√√∨	√∨	√∨

Note: √: Interceptor efficiency and ∧: Efficiency is increasing and ∨: Efficiency is decreasing.

8. Conclusions

This article tried to undertake a more accurate study of the interceptor phenomenon, by examining the effect of vertical obstacle (interceptor) at the end of a 2-D flat plate. The results from RANS equations simulation were compared with laboratory results (LOC), to the possible extent. The bottom of high speed crafts is almost flat and that's why the results of the interceptor's effect on the bottom of the flat plate can be almost the same as planing boats. This research is aimed at detailed surveys to completely understand the interceptor phenomenon. Results are briefly shown below:

(1) For numerical analysis of the boundary layer problems, the grid generation requires to be well ordered due to its sensitivity.

(2) The obtained results by finite volume algorithm should be independent of the number of elements on the grid generated, although by increasing the number of elements, more accuracy may be obtained. However, the increase of the elements number will not always lead to more accuracy, and based on the variation of the accuracy, the number of elements should be selected through trial and error to avoid extra calculation.

(3) Due to the contact of fluid flow with the plate inside the fluid, a high force of pressure is created at the point of the contact. By passing this point towards the bottom of the craft, pressure distribution decreases and causes a nonsymmetrical pressure distribution at the bottom of the plate. This nonsymmetrical pressure distribution is the main cause of trim in the crafts.

(4) The existence of interceptor creates an obstacle in the direction of flow, causing a stagnation region at the end of the flat plate.

(5) Interceptor creates vortices in front of itself. These vortices cause a hydrodynamic pressure on the bottom of the plate and consequently the pressure at the end of the plate increases, leading to changes in pressure distribution.

(6) The circulation intensity of vortex formed before the interceptor is directly related to the interceptor's height, and as the height of the interceptor increases, the pressure distribution has a local maximum at the end of the plate.

(7) Pressure distribution increase near the interceptor results in a rise in drag and lift force coefficient and if the height of the interceptor is chosen appropriately, the lift force produced is quite higher than the drag created by the interceptor.

(8) The rate of increase of the lifting force coefficient caused by the interceptor increases with the height of interceptor and attack angle, also as they increase, the amount of the lifting force increases.

(9) As a result of pressure caused at the end of the plate, interceptor makes pressure and gravity center closer to each other.

(10) Optimum choice of interceptor height has a great effect on its efficiency, and in choosing it the fluid speed must be taken into consideration, although interceptor height rise increases the lift force, speed rise may lead to a reduction in interceptor performance due to drag force increment.

(11) Interceptor is inside the boundary layer and shifts in flow speed lead to changes in boundary layer thickness, directly affecting interceptor's efficiency.

(12) In the boundary layer formed at the end of the plate, where the interceptor is, the flow speed is zero on the flat plate. Moving away from the plate, there is initially a velocity gradient whose speed increases as the distance from the plate grows. Next, after passing this velocity gradient, where distance from the flat plate is approximately 0.6 of boundary layer thickness, flow speed in the boundary layer almost equals flow speed out of the boundary layer.

(13) Speed increase leads to boundary layer thickness decrease, whereby the height of boundary layer velocity gradient also decreases, and the height of interceptor in boundary layer velocity gradient increases too, resulting in an increment in the speed of flow contact with the interceptor.

(14) While the interceptor is in the boundary layer velocity gradient, little drag is produced compared to lift force created by the interceptor, since in the boundary layer velocity gradient, flow speed is much less than the flow speed out of the boundary layer.

(15) When the interceptor's height is higher than the height of boundary layer velocity gradient, the speed of fluid contact with the interceptor is almost the same as the flow speed out of the boundary layer, and as its result, since drag force is proportionate to velocity square, it increases drastically and in spite of this rise of drag force, less lift force is produced.

Acknowledgements

The authors would like to express the deepest gratitude to Fatemeh AnavriVind for taking part in useful editing of the paper. LOC, CAPES and CNPq (Brazilian Research Agencies) are also greatly acknowledged.

References

[1] BLOUNT D. L., CODEGA L. T. Dynamic stability of planing boats[J]. **Marine Technology,** 1992, 29(1): 4-12.

[2] IKEDA Y. **Stability of high speed craft** (VASSALOS D. **Contemporary ideas on ship stability**)[M]. New York, USA: Elsevier ScienceLtd, 2000, 401-409.

[3] ZERAATGAR H., BAKHSHANDEHROSTAMI A. An investigation on ship operability versus equipment operability in irregular waves[J]. **Brodogradnja,** 2012, 63(1): 30-34.

[4] SAVITSKY D. Hydrodynamic design of planing hulls[J]. **Marine Technology,** 1964, 1(1): 71-95.

[5] ZERAATGAR H., BAKHSHANDEHROSTAMI A. and NAZARI A. A study on performance of planing-wing hybrid craft[J]. **Polish Maritime Research,** 2012, 19(4): 16-22.

[6] GHADIMI P., BAKHSHANDEHROSTAMI A. and JAFARKAZEMI F. Aerodynamic analysis of the boundary layer region of symmetric airfoils at ground proximity[J]. **Aerospace Science and Technology,** 2012, 17(1): 7-20.

[7] KARAFIATHAND G., FISHER S. C. The effect of stern wedges on ship powering performance[J]. **Naval Engineers Journal,** 1987, 99(3): 27-38.

[8] MOLINI A., BRIZZOLARA S. Hydrodynamics of interceptors: A fundamental study[C]. **Proceedings ICMRT 2005, International of Conference on Maritime Research and Transportation.** Ischia (Naples), Italy, 2005.

[9] TSAI F. J., HWANG J. L. Study on the compound effects of interceptor with stern flap for two fast monohulls[C]. **Oceans'04. MTTS/IEEE Techno-Ocean'04.** 2004, 2: 1023-1028.

[10] PELÁEZ G., MARTÍN E. and LAMAS A. M. et al. Preliminary study of a new stern device to improve efficiency in a fishing craft[C]. **First International Symposium on Fishing Craft Energy Efficiency.** Vigo, Spain, 2010.

[11] BRIZZOLARA S. Hydrodynamic analisys of interceptor with CFD method[C]. **Proceedings of FAST 2003: The 7th International Conference on Fast Sea Transportation.** Ischia, Italy, 2003.

[12] De LUCA F., PRANZITELLI P. A. Experimental and numerical investigation on interceptors' effectiveness[J]. **Proceeding HPER 10.** Melbourne, Australia, 2010.

[13] BRIZOLARA S., VILA D. A systematic CFD analysis of falaps/interceptor hydrodynamic performance[C]. **Proceedings 10th International Conference on Fast Sea Transportation (FAST 2009).** Athens, Hellenic, 2009.

[14] MARITIME DYNAMICS INC. Interceptors/trim tabs/ force producers for ship motion control[R]. MDI Report, Lexington Park, Maryland 20653, availablefrom http://maritimedynamics.com/interceptor.pdf, 2010.

[15] GHASSEMI H., MANSOORI M. Interceptor hydrodynamic analysis for handling trim control problems in the high-speed crafts[J]. **Journal of Mechanical Engineering Science,** 2011, 225(11): 2597-2618.

[16] WANG Fu-jun. **Analysis of computational fluid dynamics: Principle and application of CFD software**[M]. Beijing, China: Tsinghua University Press, 2004(in Chinese).

[17] FLUENT. **FLUENT 13**[S]. New Hampshire, USA: Users Guide. Fluent Inc., 2013.

[18] VERSTEEG H. K., MALALASEKERA W. **An introduction to computational fluid dynamics. The finite volume method**[M]. Harlow, England, UK: Prentice-Hall, 2000.

[19] XING T., STERN F. Factors of safety for Richardson extrapolation[J]. **Journal of Fluids Engineering,** 2010, 132(6): 061403.

[20] MACHADO L. V., FERNANDES A. C. Model testing and CFD analysis of 2-D profiles toward offshore application[C]. **ASME 2013 32nd International Conference on Ocean, Offshore and Arctic Engineering.** Nantes, France, 2013.